Egyptian Journal of Chemistry

Study of CeO₂@ TiO₂/ POM and CoFe₂O₄@ SiO₂ / POM Composites as Highly Efficient Eco-friendly Anti-Corrosion Coating for 316 Stainless Steel

Naglaa.M. Nooredeen* [1], Elham. A. Youssef [1], Abdel-Rahman. M. Mousa[2], Mahmoud. A. Abd El-Ghaffar* [1]

[1] *Polymer and Pigments Department, National Research Centre, 12622, Cairo, Egypt*
[2] *Chem. Dep. Faculty of Science, Ain Shams University, Abbasia, 11566, Cairo Egypt.*

Abstract

In this study, composite coatings based on metal phosphomolybdate (POM) core-shells were synthesized for enhancing and protecting Stainless Steel 316. The structures of CeO₂@ TiO₂/ POM and CoFe₂O₄@ SiO₂ / POM particles were studied and confirmed via spectrophotometric measurements e.g., X-ray Diffraction (XRD) and Atomic Force Microscope (AFM), in addition to, Transmission and Scanning Electron microscopes (TEM & SEM). The Corrosion tests of the powder pigments of all composites, and epoxy-based paint films of CoFe₂O₄@SiO₂ / POM were examined by Potentiodynamic Polarization Curve (Tafel), and electrochemical impedance spectroscopy (EIS) to evaluate the anticorrosion performance of the composites. The powder pigments and the paint films of the examined composites achieved good corrosion protection properties of the examined composites according to the electrochemical studies as follows: for powder pigment, Vanadyl - > Bismuth- > Manganese - > Zirconyl - POM/ CeO₂@ TiO₂ core-shell, and for paint films Zirconyl- > Vanadyl -> Bismuth- CoFe₂O₄@ SiO₂ / POM.

.

1. Introduction

Corrosion is an electrochemical oxidation of metal that occurs naturally when it comes into contact with an oxidant such as oxygen, hydrogen, or hydroxide. Typically, this kind of damage results in metal oxides or salts. In numerous industrial domains, corrosion is a major issue [1-3]. Through a variety of methods, including cathodic protection, anodic protection, the use of corrosion inhibitors, and the application of barrier coatings to metal surface, corrosion that can be prevented to some extent [4,5].The performance of materials in buildings such as their strength, aesthetics, and permeability to liquids and gases, decrease due to corrosion. The necessity for better corrosion management systems has increased due to the total economic impact of corrosion on industrial and home applications. More than US $3 trillion is thought to be the annual cost of corrosion, or around 3.4% of the global Gross domestic Product (GDP). However, by applying corrosion inhibitors, coatings, electroplating, and other corrosion control methods, current corrosion mitigation procedures have predicted yearly savings of 15–35% of the corrosion cost.

A corrosion inhibitor is frequently utilized as a corrosion prevention as it is simply to apply and for its relatively low cost [5-9].

Corrosion inhibitors can either adsorb on metal surfaces or interact with corrosion byproducts like metallic ions to create insoluble complexes that greatly slow down additional corrosion reactions.

There are restrictions on the creation and use of corrosion inhibitors; nano-particles are incorporated in coatings to enhance their chemical, mechanical, and optical characteristics. Nano-coatings are used successfully to decrease the effects of corrosive environments since they possess several advantages including surface **hardness**, adhesive quality, as well as resistance to corrosion at high temperatures.

Aside from that, current research suggests that adding nanoparticles to coating systems improves protection because they act as fillers, reduce porosity, and change the layer's barrier characteristics [10–13]. In order to improve wear, corrosion resistance, mechanical qualities, and high barrier protection properties in the coatings, particles like TiO₂, SiO₂, Fe₂O₃, CeO₂, Al, ZnO, and Al₂O₃ with some surface modifications have been utilized [14–17].

These nanoparticles can cover the minuscule gaps and empty spaces that occurred in the coating matrix because of their small size and large surface area, lengthening the electrolyte channel. The corrosion protection behavior of nanotechnology was reported in a previous study by Shen et al. [18] about the corrosion-prevention performance of nano-TiO_2 coatings on 316 L stainless steel in both dim and UV illumination conditions. The coating demonstrated outstanding corrosion resistance during testing in a 0.5 molL^{-1} NaCl solution because it functioned as a ceramic barrier on the metal's surface. This was supported by the finding that for stainless steel coated with TiO_2 nanoparticles, the corrosion current density was reduced by three orders of magnitude and the corrosion resistance was increased by more than a hundredfold when compared to uncoated steel. Mahmoud et al. [19] also reported that the TiO_2 layer deposited on weathering steel displayed higher corrosion resistance properties than the bare steel in NaCl aqueous solution, under UV light.

In a previous study it was reported that, the incorporation of $CoFe_2O_4$-SiO_2 nano-pigment into the epoxy coating resulted in a significant improvement of the coating corrosion protection properties, and was found that $CoFe_2O_4$-SiO_2 nano-pigment, due to proper dispersion, could fill the cavities and block the electrolyte pathways [20, 21].

The ultimate goal of this study is to Prepare, characterize and evaluate the novel nano composite pigments of $CeO_2@$ $TiO_2/$ POM and $Co_2Fe_2O_4@$ SiO_2 / POM composites as corrosion inhibitors for 316 L Steel to be applied for coating applications from the economic and environmental point of view.

2. Materials and Methods

2.1. Materials and reagents

All chemicals were of analytical grade and used without further purification. $H_3PMo_{12}O_{40}.xH_2O$, $ZrOCl_2.8H_2O$, $(NH_4)_6Mo_7O_{24}·2H_2O$, HNO_3, $VOSO_4$. $8H_2O$, $MgCl_2.6H_2O$, $MnCl_2.4H_2O$, $AlCl_3.6H_2O$, $AlCl_3.6H_2O$, $NaCl.6H_2O$, Co $(NO_3)_2.6H2O$, Fe $(NO_3)_3.9H20$, NaOH, ethanolamine $HOCH_2CH_2NH_2$, and sodium chloride NaCl were purchased from Sigma-Aldrich, and $Na_2HPO_4·7H_2O$ from Fluka. Cerium-nitrate hexa-hydrate $(Ce(NO_3)_3·6H_2O)$, Potassium hydroxide (KOH), Titanium tetra iso-propoxide (TTIP), Isopropanol, Hydrochloric acid. Tetraethyl orthosilicate (TEOS) $SiC_8H_{20}O_4$ was also from Sigma-Aldrich. Two components solvent-free epoxy resin (NPEL-128, a product of NAN YA Plastic Corporation, Taiwan) was used in this study as the main binder for all paint formulations prepared in this study. The epoxy equivalent of epoxy resin is 184-190 g/eq, and the mixing ratio of Epoxy Resin to Hardener is (100:60) by weight.

2.2 Instrumentation

A Metrohm pH/ Ion-meter Model 692 with a combined glass pH electrode Model Metrohm 6.0202.100 was used for all pH measurements. Surface morphology of the prepared samples was analysed using Scanning Electron Microscope (SEM) Model JSM 6360LV, JEOL/ Japan. The Energy Dispersive X-ray spectrometer (EDX) attached to the microscope was utilized for elemental analysis. Transimition Electron Microscope (TEM) JEM-2100Plus is a multi- purpose transmission electron microscope for micro structure evaluation; the images obtained using an accelerating voltage of 20 kV. Philips 133 X-ray diffractometer (PW 1930 generator, PW 1820 goniometer) equipped with Cu Kα radiation 134 (45 kV, 40 mA). The electrochemical measurements performed using electrochemical workstation CH Instruments Inc. (CHI 660D) with a platinum counter electrode and Ag/AgCl/Cl$^-$ reference electrode filled with 1 M KCl, the working electrode was glassy carbon electrode GCE.
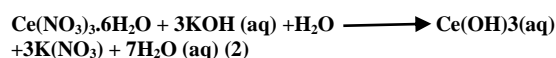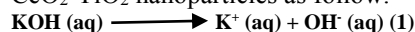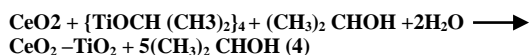
2.3 Preparation of CeO$_2$ Core[22]

The preparation of ceria (CeO_2) NPs was carried out as following process: Cerium-nitrate hexa-hydrate $(Ce(NO_3)_3·6H_2O)$ and potassium hydroxide (KOH) were taken in 1:4 molar ratios and completely dissolved in deionized water. After that, the solution pH value was adjusted to be 12. Then, the mixed solution was stirred with a magnetic stirrer for 4 hours until precipitation is formed. The prepared precipitate was filtered several times with water and ethanol. Later on, the filtered sample was dried in oven at 80ºC for about 30 minutes. The synthesized powder was annealed at 500 ºC for 2 hours, forming finally, the CeO_2 NPs.

2.4. Synthesis of CeO$_2$-TiO$_2$ Core-shell Nanoparticles [22]

In the typical wet chemical method of core-shell nanoparticles, initially 0.3g of CeO_2 is dispersed in isopropanol by using ultra-sonicator. The ultra-sonicated solution is stirred by using a magnetic stirrer with a rate of 700 rpm for 1hr, later on; 6ml of TTIP is added to the dispersed ceria solution.

As TiO_2 is unstable in the nano level, so a few drops of diluted hydrochloric acid are added in order to adjust the pH 1, and to stabilize TiO_2 nanoparticles. Then the solution is stirred for 12 hrs and dried at 100°C for 1h. The obtained nanoparticles are annealed at 500°C to get CeO_2-TiO_2 NPs. The reaction mechanisms are presented here for attaining CeO_2-TiO_2 nanoparticles as follow:

$$KOH \ (aq) \longrightarrow K^+ \ (aq) + OH^- \ (aq) \ (1)$$

$$Ce(NO_3)_3.6H_2O + 3KOH \ (aq) + H_2O \longrightarrow Ce(OH)3(aq) + 3K(NO_3) + 7H_2O \ (aq) \ (2)$$

$$2Ce(OH)_3 (aq) \longrightarrow 2CeO_2 + H2O (aq) (3)$$

$$CeO2 + \{TiOCH (CH3)_2\}_4 + (CH_3)_2 CHOH + 2H_2O \longrightarrow$$
$$CeO_2 - TiO_2 + 5(CH_3)_2 CHOH (4)$$

2.5. Synthesis of POM- CeO₂-TiO₂ Core-shell Nanoparticles

Equal amounts of the dry powder of the previously prepared CeO₂.TiO₂ NPs were mixed with the desired POM dry powder, followed by ultra-sonication in order to be well homogenised before use.

2.5.1. Preparation of Bare, CeO₂.TiO₂ Core-Shell NPs, and POM- CeO₂.TiO₂ Core-Shell NPs Electrodes

Prior to the modification, GCE electrode was mechanically polished with wetted micro-cloth containing alumina slurry and washed with distilled water for 2-3 times and allowed to dry at room temperature. Then, 10μg of CeO₂.TiO₂ CSNPs were dispersed in 2μg of isopropanol and 3μg of double distilled water by ultrasonication. Then, the prepared suspension was dropped on the GCE electrode and left to dry for 1hr at room temperature.

2.6. Preparation of CoFe₂O₄@SiO₂[23]

Magnetic nano-spheres (0.15 gm) of CoFe₂O₄ were added to 50 mL EtOH (80%) and dispersed under ultrasound conditions for 30 min. Afterward, the pH of the mix should be 11–12 where NH₃.H₂O solution should be added to increase the pH of the mixture to 11–12. In the next step, 2 mL of Tetraethyl orthosilicate (TEOS) was added drop by drop into the mixture with vigorous stirring at 25 °C for 20 h. Then, by an external magnet, the grey CoFe₂O₄@SiO₂ powder synthesized was separated and washed with deionized water. Subsequently, at 80 °C, CoFe₂O₄@SiO₂was dried for 10 h.

2.7. Synthesis of POM- CoFe₂O₄ @SiO₂ Core-shell Nanoparticles

Equal amounts of the dry powder of the previously prepared CoFe2O4@SiO2 NPs and POM dry pigment were mixed by ultrasonication and well homogenised before use.

2.8. Preparation of Bare, CoFe₂O₄@SiO₂ Core-Shell NPs, and POM/ CoFe2O4@SiO2 Core-Shell NPs Electrodes

GCE electrode was mechanically polished with wetted micro-cloth containing alumina slurry and washed with distilled water for 2-3 times and allowed to dry at room temperature. Then, 10μg of CoFe₂O₄@SiO₂ and POM/CoFe₂O₄@SiO₂ CSNPs were dispersed in 2μg of isopropanol and 3μg of double distilled water by ultra-sonication. Then, the prepared suspension was dropped on the GCE electrode and was left to dry for 1hr at room temperature.

2.9. Steel Substrate Preparation

Stainless steel SS 316L with a nominal chemical composition of Fe, Ni, Cr, Si and C was used as the substrate. The samples were machined to dimensions of 10 cm × 6 cm. All specimens were cleaned using an ultrasonic bath over three rinsing steps (detergent solution, distilled water, and acetone) to remove any organic residuals.

2.10. Coating of the paint-containing pigments onto Stainless steel panels

The Stainless Steel substrates were chemically treated with 5% H₂SO₄ at room temperature, in order to remove any corrosion products on the surface, and then thoroughly rinsed with distilled water. Further, it was washed with acetone to remove any oil, grease or any other organic contaminants before the application of paint which was done by Standard methods used to apply paints to structural steelwork such as application by paint brush, or roller.

2.11. Painting technique

After the substrate is properly cleaned and dried, it is then ready for the painting process. In order to reduce the duration of painting process, we employed" wet on wet" technique. In this technique, one coat is painted then the next coat is immediately applied perpendicular to the first coat. To achieve optimum and similar coatings, painting process is conducted in temperature ranges between 25 - 30°C. After painting, the coated steel samples were left to dry at ambient temperature for 3-4 hours.

2.12. Preparation of Paint with different pigments

The synthesized pigments were finely grinded for 45 min, and then the epoxy resin and solvent were added to it and were grinded all together using stainless ball mill for 2 h until very fine paint dispersion was obtained. Ball Mills are used wherever the highest degree of fineness is required in addition to well-proven mixing and size reduction processes. The different paints composition is given in Table 1.

3. Results and Discussion

Phosphomolybdate (POMs) of Bismuth, Manganese, Vanadyl and Zirconyl were synthesized using precipitation method from acidified aqueous media. The core-shell structures were prepared using the method mentioned above. Each composite of the prepared phosphomolybdate pigment with either core-shell was prepared in the 2:1 ratio. All the prepared materials were characterized using microscopic and electrochemical techniques. The synthesised materials were investigated for their anti-corrosive efficiency.

_____

Table 1. Composition of the prepared paints using different pigments of POMs, core-shell $CoFe_2O_4@SiO_2$ and their corresponding $POM/CoFe_2O_4@SiO_2$ nanocomposites

Sample	Pigment and extenders				Synthesized Anticorrosive Pigments			*Epoxy resin and hardener	Solvent*	Total
	ZnO	TiO2	Talc	Baryte	M-POM	CoFe2O4@SiO2	M-POM / CoFe2O4@SiO2			
I	15	12	12	13	5	-	-	25	18	100
II	15	12	12	13	-	5	-	25	18	100
III	15	12	12	13	-	-	5	25	18	100

Abbreviations: M= $(ZrO)^{2+}$, Mn^{2+}, Bi^{3+} and $(VO)^{2+}$ * The solvent used was Xylene: Ethyl Acetate: Isopropanol (6:3:1) mixture. All values are given in grams for solids and in millilitres for solvents

3.1 Electron Microscopic Characterization: SEM and TEM

The morphology of $CeO_2@TiO_2$ particles was examined by SEM at different magnifications, as shown in **Fig. 1.** The SEM photos showed the spherical morphology of $CeO_2@TiO_2$ particles fused to each other's. However, TEM images in **Fig. 2** showed a core-shell structure of the prepared nanoparticles, although a large amount of aggregation is observed, the particles sticking together to form clumps and aggregates which are then coated with the SiO_2. According to TEM, the particles range in size from approximately 15.2 nm in the core, with the coatings (shell) being approximately 26.8 nm in thickness. This gives the particles a total size of ≈ 40 nm. Although these images do not show the ideal structure of a single core contained within a shell, they confirm the formation of the required core-shell silica-cobalt ferrite nanoparticles. As shown in **Fig. 3,**

the prepared $SiO_2@CoFe_2O_4$ NPs have uniform size with narrow size distributions. It can also be seen that these NPs have core-shell structure and good dispersity. Their core-shell structure is the indirect evidence to verify the formation of silica shell on the surface of $CoFe_2O_4$.

3.2. Atomic Force Microscopy (AFM)

Surface morphology of the synthesized materials was characterized by performing Scanning Probe Microscopy SPM analysis using Agilent 5600LS AFM, High-Resolution Large Stage AFM working in contact mode. **Fig.4(A)** shows topographical images at a high resolution, where, the brightness of the white areas of the image corresponds to the height, allowing for qualitative distinction of the small and large particles. A uniform and characteristic cube-like structure was observed for $CeO_2@TiO_2$ nanoparticles, as clearly seen **in Fig.4(B),** which shows the three-dimensional (3-D) enhanced images of A
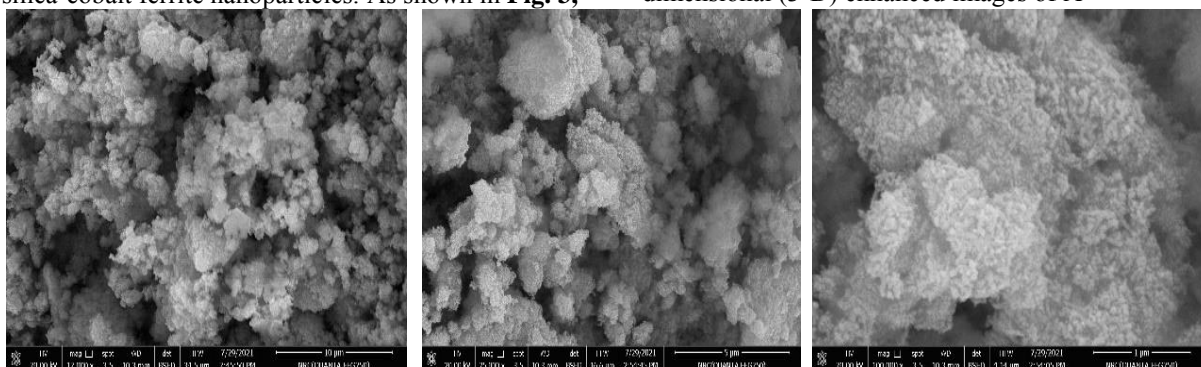
Fig. 1. SEM of $CeO_2@TiO_2$ nanoparticles
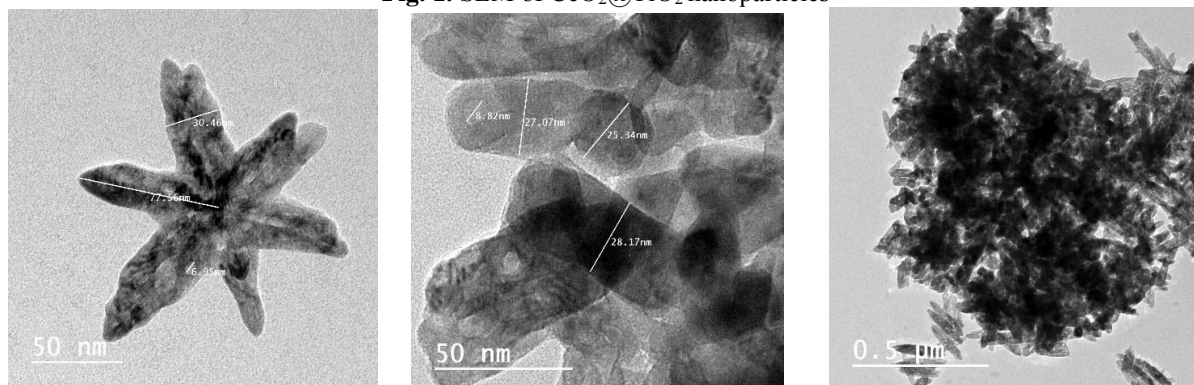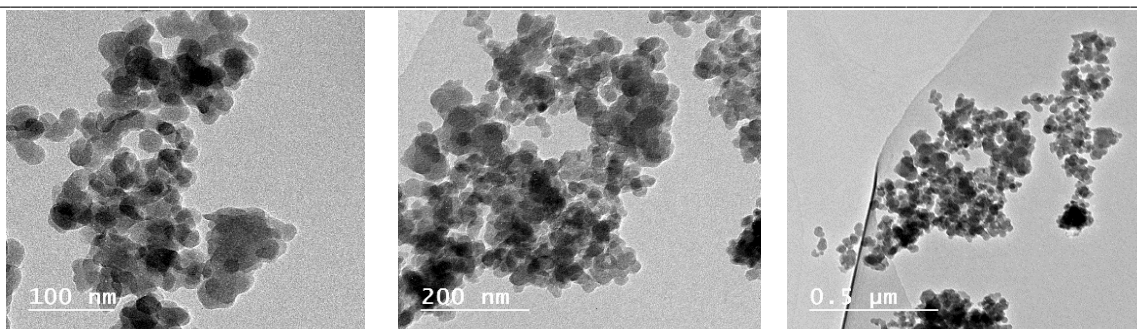

Fig. 2. TEM of $CeO_2@TiO_2$ nanoparticles

_____

Fig. 3. TEM of CoFe$_2$O$_4$@SiO$_2$ nanoparticles
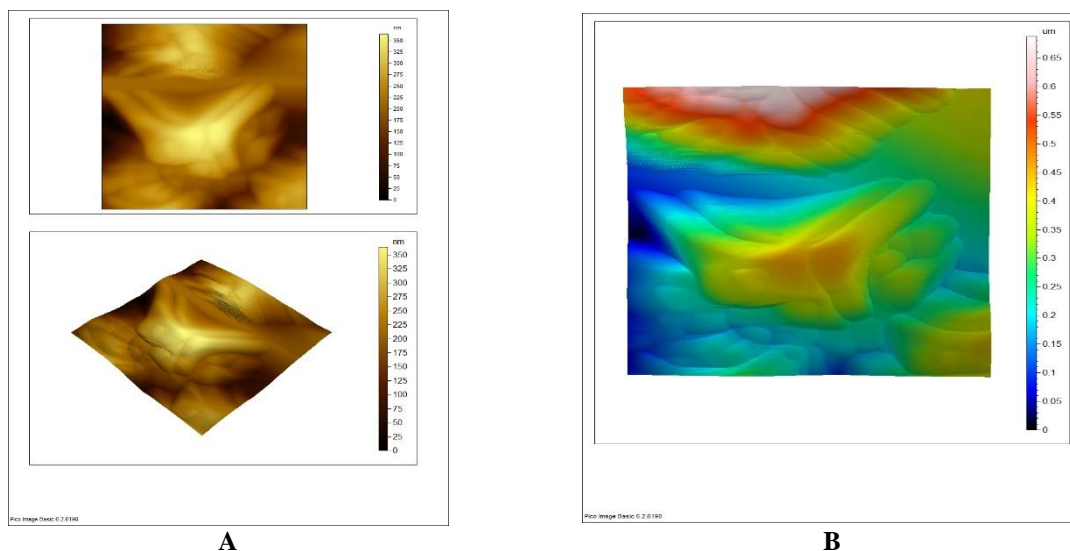
.

A   **B**

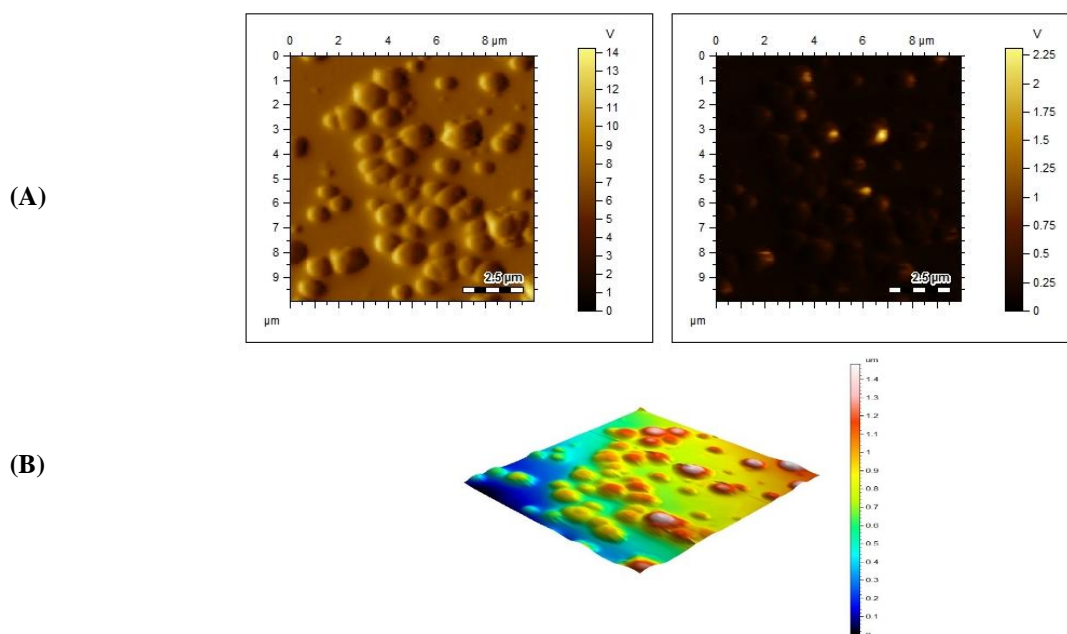**Fig. 4.** AFM images, two dimentional topograhical (A) and three dimensional topographical (B) of CeO$_2$@TiO$_2$

(A)

(B)

Fig. 5. AFM images of CoFe$_2$O$_4$@SiO$_2$ -(VO)$_3$(PMo$_{12}$O$_{40}$)$_2$

Figure 5 shows high-resolution CM-AFM images of nanoparticles $CoFe_2O_4@SiO_2$-$(VO)_3$ $(PMo_{12}O_{40})_2$. High-resolution topographical images are displayed in **Fig 5(A)**, and the height-dependent brightness of the white portions of the image enables the qualitative separation of tiny and large particles. The core-shell nanoparticles were found to have a consistent and recognized cube-like structure. The Vo-POM particles with larger size development of nanoparticles, **Fig 5 (B),** illustrates the three-dimensional (3-D) enhanced images of the $CoFe_2O_4@SiO_2$-$(VO)_3(PMo_{12}O_{40})_2$ nanocomposite that was confirmed from the small particles seen surrounding and over the core-shell particles.

3.3 X-Ray Diffraction (XRD) Spectroscopy

In this work, the XRD patterns of cobalt ferrite-NPs and its corresponding M-POM nanocomposites were carried out using a Philips 133 X-ray diffractometer (PW 1930 generator, PW 1820 goniometer) equipped with Cu Kα radiation 134 (45 kV, 40 mA). The scans were run in *2θ r*ange of 5º to 80º with a step size of 0.02 and step time of 1*s*. The average crystallite size was calculated from the most intense peak by using Scherrer's formula $X_d = k \lambda / \beta \cos \theta$, where $k = 0.9$ is the Scherrer's constant, $\lambda = 1.54056$ Å is the wavelength of X-ray, and D is the full width at half-maximum intensity (FWHM) of the peak.

As shown in Fig. 6, the peaks centered at 27.4, 36.1, 44.01, and 54.3 correspond to the (101), (004), (200), and (211) reflections of rutile TiO_2. Moreover, the (111), (200), and (220) planes of CeO_2 cubic structure could be responsible for the peaks at 27.4, 33.3, and 46.4. Figure 6 showed TiO_2 and CeO_2 peaking. Because the amount of CeO_2 was so much less than for TiO_2, the intensity of the CeO_2 peaks in Fig. 6 is slightly weaker than it could be. These results allowed us to deduce that rutile TiO_2 and cubic fluorite CeO_2 may form at500°C and that our method could be used to produce the TiO_2/CeO_2 composite. Applying Scherrer's method to calculate the average size of crystallizations, it is clear that the presence of CeO_2 reduces the crystallite size, which is 25.4 nm for pure TiO2 versus 8.5 nm for the hydrothermal synthesis of TiO_2/CeO_2. According to previous studies, the composition of CeO_2 prevented the rutile phase from growing. As shown in Fig. 6, the XRD reveals the existence of Ce 9.1%, Ti 53.3%, and O 37.3%.

The XRD pattern of SiO_2-coated $CoFe_2O_4$ nanoparticles is shown in Fig 6. The dominating peaks present those of $CoFe_2O_4$. The broad peak at low angles may indicate the presence of the SiO_2. By comparison with the JCPDS Joint Committee on Powder Diffraction Standards database for SiO_2 and the results obtained by pervious work, the peak at 2Θ = 27 contains a trace of SiO2 along with the peak at

$2\theta \approx 35$, however both of these peaks are highly masked by the $CoFe_2O_4$ peaks in the same area. The XRD result shows that the elemental composition of CoFe2O4/SiO2 NPs is, Fe is 0.7 %, Co is 0.4 %, O is 53%, and Si is 46 %.
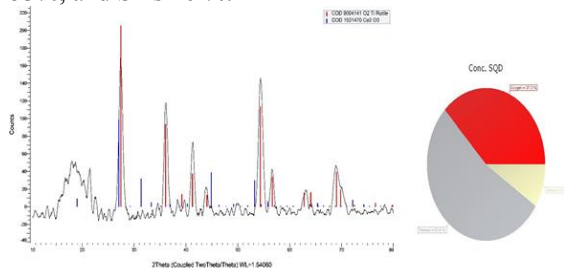

Fig. 6. XRD of $CeO_2@TiO_2$ nanoparticles

Fig.7. XRD of $CoFe_2O_4@SiO_2$ nanoparticles

On the other hand, XRD of $CoFe_2O_4@SiO_2$-$(VO)_3(PMo_{12}O_{40})_2$ Fig. 8 shows and proves the formation of new composite material between the VO-POM and the core-shell $CoFe_2O_4@SiO_2$. The XRD result show that the elemental composition % of VO-POM@ $CoFe_2O_4/SiO_2$ NPs is Fe 1%, Co 0.5 %, O 36.6 % and Si 15.2 %., P 30.5%, V 1.1% and Mo 15.2%.

3.4. Corrosion Studies

3.4.1. Open circuit potential (OCP)

The OCP change (potential vs time) graphs [21] for Bare steel, Bare GCE electrode, $CeO_2@TiO_2$ Core-Shell, Mn-POM/ $CeO_2@TiO_2$ Core-Shell, Zr-POM/ $CeO_2@TiO_2$ core-shell, VO-POM/$CeO_2@TiO_2$ core-shell, $CoFe_2O_4@SiO_2$, ZrPOM/$CoFe_2O_4@$ SiO_2 core-shell, MnPOM/ $CoFe_2O_4@SiO_2$ core-shell, VOPOM/ $CoFe_2O_4@SiO_2$ core-shell and BiPOM/ $CoFe_2O_4@SiO_2$ core-shell nanocomposites deposited on SS coupons in 3.5 wt % NaCl solution at 25-30 °C temperature for an 400,800 s immersion duration is shown in Figs. 9 and 10.
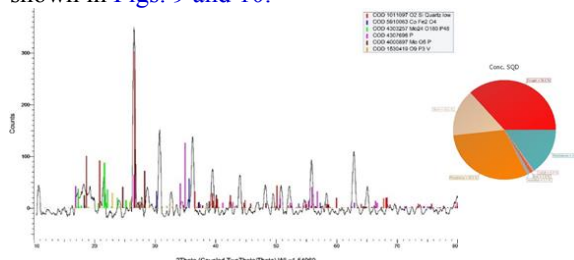

Fig. 8. XRD of $CoFe_2O_4@SiO_2$ - $(VO)_3(PMo_{12}O_{40})_2$ nanoparticles.

These curves demonstrated that the time was adequate to achieve steady-state potential. The M-POM / Core-shell nanocomposite coatings produce a positive shift in OCP when compared to blank, with the maximum positive shift occurring in the case of the VO-POM/ core-shell [$CeO_2@TiO_2$, $CoFe_2O_4@SiO_2$] nanocomposite coating. This indicates the highest level of protection provided by the Mn and VO-POM/ core-shell, $CeO_2@TiO_2$, $CoFe_2O_4@SiO_2$ nanocomposite coating.

The more positive shift in the values of OCP indicates their high corrosion resistance, which is a result of both the barrier and the passive oxide layer effects at the metal/coating interface. The presence of SiO_2 and TiO_2 in the nanocomposite coating has shifted the potential in a more noble direction and improved the coating's redox behavior and barrier characteristics. The higher corrosion protection ability of the M-POM / $CeO_2@TiO_2$ and M-POM $CoFe_2O_4@SiO_2$ nanocomposite coatings over $CeO_2@TiO_2$, $CoFe_2O_4@SiO_2$ and M-POM for the full immersion time is due to the superior barrier effect which changes resulting from the formation of a more adhesion, denser and uniform layer on the steel surface. Initially, corrosive ions penetrate the coating and reach the surface of the steel, leading to anodic dissolution of metal and consequently a decrease in potential. Then formation of a passive oxide layer on the coating/steel surface.

3.4.2. Electrochemical Impedance Spectroscopy (EIS)

The EIS experiments were carried out using an electrochemical workstation Model (CHI 660D) CH Instruments Inc., equipped with a three-electrode electrochemical cell, where a bare and/or coated glassy carbon electrode (GCE) was used as the working electrode, a Platinum wire as the counter electrode and Ag/AgCl/ Cl⁻ as the reference electrode. The measurements were carried out in a frequency range from 10^{-2} to 10^5 Hz with AC amplitude of 10 mA. EIS [24a,b] was used to evaluate the anti-corrosion performance of the synthesised composites and compare it to both their corresponding POM and by interpretation of its result using both Nyquist and Bode presentations.
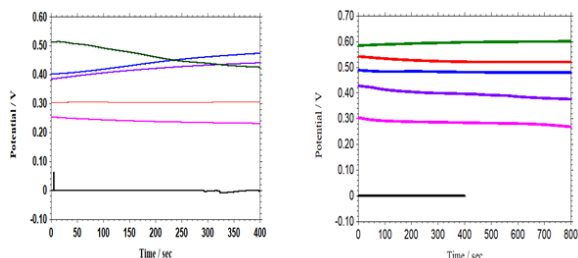

Fig. 9. OCP of **(A)** Bare electrode (black), $CeO_2@TiO_2$ core-shell (pink), Mn-POM/ core-shell (red), Zr-POM/ core-shell (violet), VO-POM/ core-

shell (green), Bi-POM/ core-shell (blue) **(B)** Bare electrode (black), $CoFe_2O_4@SiO_2$ (pink), ZrPOM/ core-shell (violet), MnPOM/ core-shell (red), VOPOM/ core-shell (green) and BiPOM/ core-shell (blue). The OCP was measured between reference electrode and working electrode in artificial seawater (3.5% NaCl).
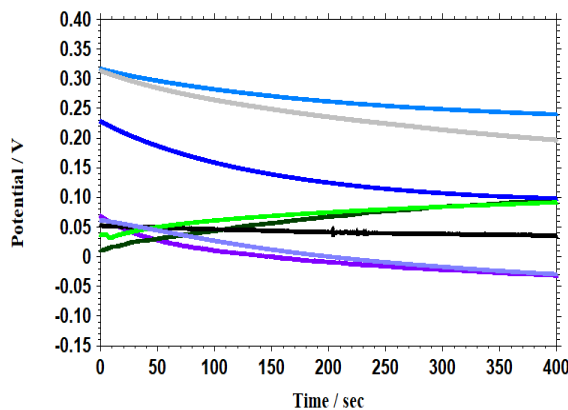

Fig. 10. OCP of $CoFe_2O_4@SiO_2$- (black), ZrPOM/ core-shell (violet), VOPOM/ core-shell (green) and BiPOM/ core-shell (blue), - epoxy–Stainless Steel, $CoFe_2O_4@SiO_2$- (grey), ZrPOM/ core-shell (pale violet), VOPOM/ core-shell (pale green) and BiPOM/ core-shell (pale blue), - epoxy –Stainless Steel after 3 weeks of immersion in 3.5% NaCl. The OCP was measured between reference electrode and working electrode in artificial seawater (3.5% NaCl).

3.4.2.1. EIS of POM/ Core-Shell Composite Paints on Stainless Steel Substrates [25a,b]

The prepared paints containing POMs and their corresponding POMs/ core-shell nano-composites were applied onto stainless steel plates then investigated by EIS. The obtained EIS parameters measured in 3.5 % NaCl solution before and after performing corrosion test are shown in Table 2. The data in Table 2 shows that the R_{ct} values obtained for ZrO-, Bi- and VO-POM/ $CoFe_2O_4@SiO_2$ composites-based paints applied onto SS plates are higher compared to their corresponding POM-based paints. The estimated R_{ct} values of the above mentioned composites were found to be 53 MΩ cm², 29 MΩ cm² and 12 MΩ cm² respectively, compared to 410 kΩ cm², 260 kΩ cm² and 15 kΩ cm² for their corresponding POMs and 5.1 kΩ cm² for $CoFe_2O_4@SiO_2$. This result reveals the enhanced anti-corrosion power achieved by the application of the paints containing the developed composites. The R_{ct} values measured for the coated SS plates were found to be higher than those estimated for the corresponding materials measured using GCEs due to the nature of the conductivity of the plates, as shown in Fig.11 (A, B) for both types of $CeO_2@TiO$, and $CoFe_2O_4@SiO_2$ core-shell particles.

Table 2. Electrochemical parameters obtained by EIS measurements of the POMs and their composites with core-shell $CoFe_2O_4@SiO_2$, applied on Stainless Steel plates and measured in 3.5 % NaCl solution.

Type of paint / Property		Bare metal	CoF@S	ZrO-POM	ZrO-POM/CoF@S	Bi-POM	Bi-POM/CoF@S	VO-POM	VO-POM/CoF@S
R_{ct} (kΩ cm²)	B	$1\ 10^{-5}$	$8.1\ 10^6$	$4.1\ 10^2$	$5.3\ 10^4$	260	7.423	15	0.210
				$1.4\ 10^2$	$2.1\ 10^2$	59	$2.3\ 10^2$	1	0.1494
	A	------	----	1.616	$3.1\ 10^9$	$1.6\ 10^4$	$1\ 10^9$	$1.3\ 10^3$	$1.2\ 10^4$
				$2.1\ 10^3$	$2.2\ 10^4$	1	$2.9\ 10^4$	0.861	7.672
C_{dl} (μF)	B	8.9	3.7	$1.1\ 10^{-4}$	$1.3\ 10^{-5}$	$1.2\ 10^{-4}$	$2.9\ 10^{-4}$	$9.3\ 10^{-5}$	$6.5\ 10^{-2}$
		------	$6.3\ 10^{-1}$	$5.2\ 10^{-4}$	$4.3\ 10^{-4}$	$1.2\ 10^{-4}$	$3.1\ 10^{-5}$	$4.6\ 10^{-2}$	$4.9\ 10^{-4}$
	A	-------	-----	$3.2\ 10^{-6}$	$9.2\ 10^{-3}$	1.3	$90\ 10^{-2}$	8.4	0.59
		-------	-------	23	54	$140\ 10^3$	78	0.19	0.5
R_{s} (Ω cm²)	B	0.013	2230	2831	$9.2\ 10^{-3}$	0.001	2593	0.005	$2.5\ 10^4$
	A	----	-----	725	$4.3\ 10^2$	0.001	377	614	28.9

B: Before and A: After immersion in 3.5% NaCl solution for three weeks; Measurements were done in 3.5% NaCl at a scan rate 1 mV/s. Abbreviations: CoF@S means $CoFe_2O_4@SiO_2$

(A)   **(B)**

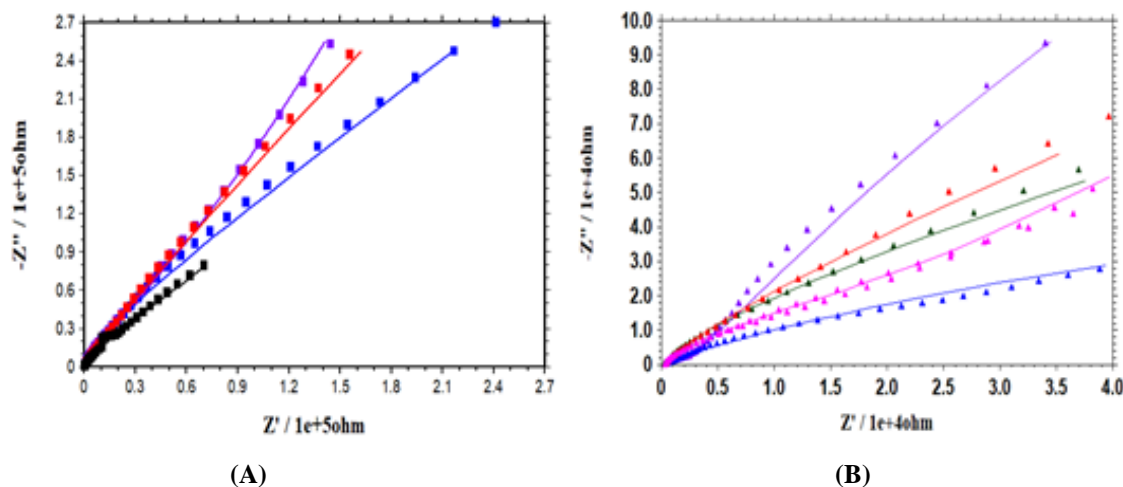**Fig. 11.** Nyquist plot of (A) Bare electrode (black), $CeO_2@TiO_2$ Core-Shell (pink), ZrO-POM/ core-shell (violet)Mn-POM/ core-shell (red), VO-POM/ core-shell (green) Bi-POM/ core-shell (blue), (B) Bare electrode (black), $CoFe_2O_4@SiO_2$ (red), VPOM/ core-shell (violet), and BiPOM/ core-shell (blue) on GCE measured in 3.5% NaCl solution at a scan rate 1mV/s.

Data in Table 2 reveals clearly that despite the considerable decrease of R_{ct} values of ZrPOM/ $CoFe_2O_4@SiO_2$ composite – based paint on SS plate from 53 MΩ cm² to 210 kΩ cm² after performing the corrosion test, it still significantly higher than the 5.1 kΩ cm² of the untreated core-shell painted Stainless Steel plate. At the same time, R_{ct} values of ZrPOM was decreased significantly from 410 kΩ cm² to 140 kΩ cm² after performing the corrosion test which is much less than the 210 kΩ cm² of the Bi- and VO-POM /$CoFe_2O_4@SiO_2$ painted Stainless Steel plate. This is obviously clear from their Nyquist plots

shown in Figs. 12 and 13 which reflect the higher anti-corrosion power of the M-POMs/ $CoFe_2O_4@SiO_2$ composite coatings compared to the POMs coatings. The decrease of R_{ct} impedance values after performing the corrosion test for all studied coatings is probably due to the penetration of water molecules and the movement of some other ions like chloride through the coatings, which more distinct in case of the POM compared to the core – shell composite coatings. This suggests that a capacitive response at the Stainless Steel/ NaCl solution interface remain effective.
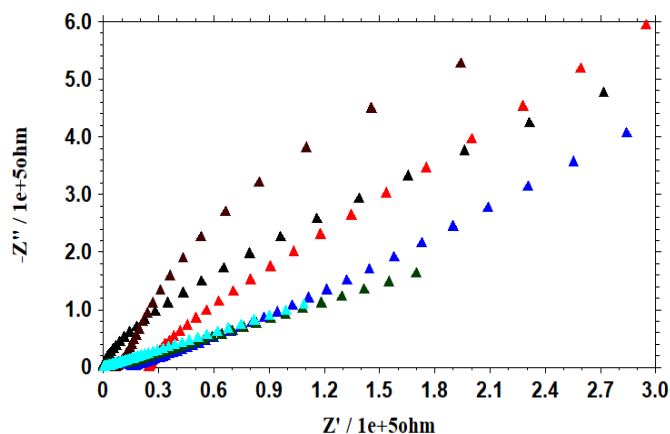
Fig.12. Nyquist plots of Bare Electrode (black), Blank (brown), VO-CoFe$_2$O$_4$@SiO$_2$ (red), VO-POM (blue), and [Vo-POM/ core-shell (green), VO-POM (light blue) after immersing in 3.5% NaCl for 3 weeks] coated on SS, measured in 3.5% NaCl solution at a scan rate 1mV/s.
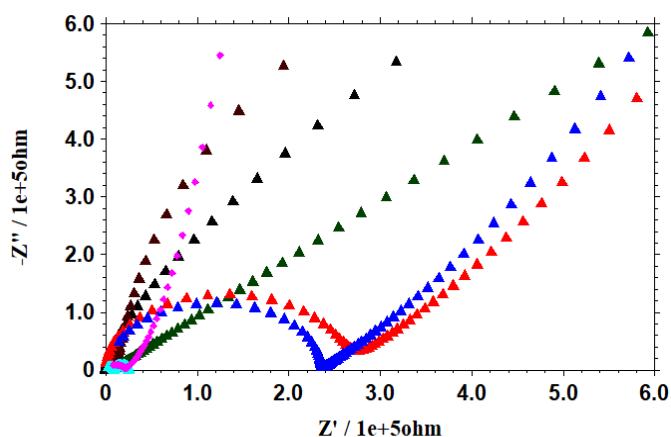

Fig. 13. Nyquist plot of Bare Stainless Steel electrode (black), Blank (brown), Bi-CoFe2O4@SiO2 (red), Bi-POM (blue), and [Bi-POM/ core-shell (green), Bi-POM (light blue), Blank (after immersing in 3.5% NaCl for 3 weeks) coated on SS, measured in 3.5% NaCl solution at a scan rate 1mV/s

.Moreover, the C_{dl} values of ZrO-, Bi- and VO-POM/ CoFe$_2$O$_4$@SiO$_2$ composites based -paints coated on SS substrates were estimated as 1.3 x10^{-5}μF, 2.9 x 10^{-4} μF and 6.5 x 10^{-2} μF respectively compared to bare 8.9 μF, as given in Table 2. The increase in R_{ct} values of the M-POM/ CoFe$_2$O$_4$@SiO$_2$ core-shell composites compared to that of the bare and CoFe$_2$O$_4$@SiO$_2$ coated SS substrates suggests a more capacitive response at the SS / NaCl solution interface due to the adsorption of more POM-Ferrite composites that work as inhibitor on the st.st surface [26]. These results reflect the improvement in the corrosion inhibition efficiency of the POM-Ferrite composites for Stainless Steel.

Figures 14 and 15 (A and B) show the Bode plots of steel coated with paint which containing Bi-, VO-POM/ CoFe$_2$O$_4$@SiO$_2$ composites respectively, before and after the corrosion test. The data calculated from this plots are presented in Table 3. Data shows that the phase angle ($θ$) for most of the paint coatings containing POM/ ferrite composites on SS substrates measured before corrosion test are close to -80 ^{o} in a wide range of frequency. After performing the corrosion test the values of the phase angle ($θ$) [27-29] of most of the coatings were decreased to about -60. Despite of that all aren't as ideal as that for Bi-, VO-POM/ CoFe$_2$O$_4$@SiO$_2$ composites; however, they still possess good anticorrosive behavior.
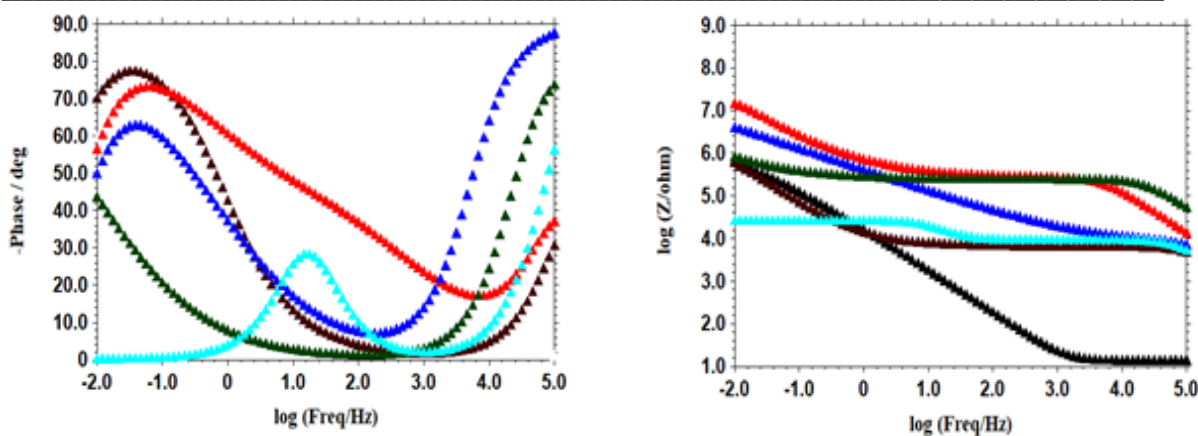
Fig.14. Bode plot of Bare Stainless Steel electrode (black), Blank (brown), Bi-CoFe$_2$O$_4$@SiO$_2$ (red), Bi-POM (blue), and [Bi-POM/ core-shell (green), Bi-POM (light blue), Blank (after immersing in 3.5% NaCl for 3 weeks) coated on SS measured in 3.5% NaCl solution at a scan rate 1mV/s.
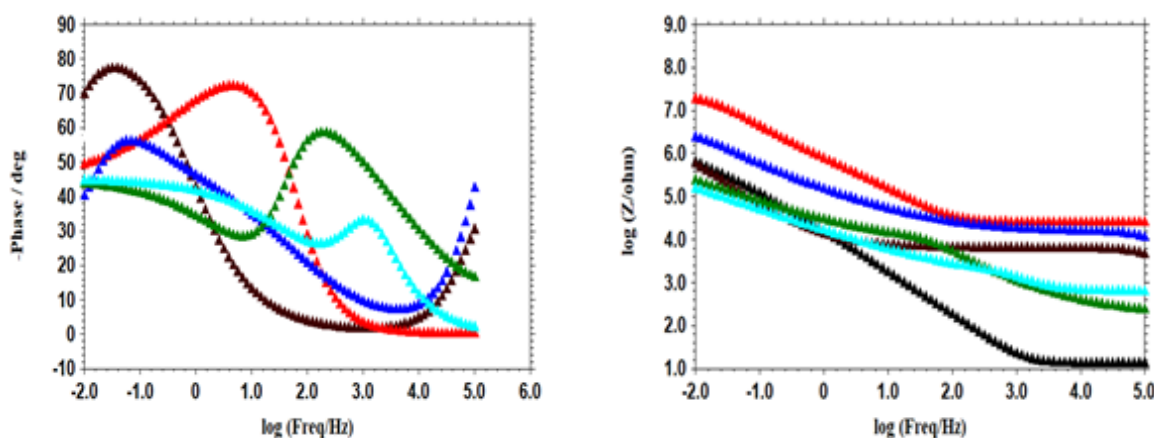

Fig. 15 Bode plot of Bare Stainless Steel electrode (black), Blank (brown), VO-CoFe2O4@SiO2 (red), VO-POM (blue), and Vo-POM/ core-shell (green), VO-POM (p. blue) after immersing in 3.5% NaCl for 3 weeks] coated on SS measured in 3.5% NaCl solution at a scan rate 1mV/s.

3.4.3. Potentiodynamic polarization (Tafel)

Potentiodynamic polarization (Tafel) [30] is a term describing the measured change in the electrical potential (voltage) of a system. The Tafel refers to a polarization technique in which the potential of the electrode is varied over a relatively large potential domain at a selected rate by the application of a current through the electrolyte. The polarization curves were conducted at a scan rate of 10 and 1 mV/s using a GCE or coated steel plate with 1.0 cm2 area of operating electrode in solution of 3.5% NaCl. Table 3 shows the polarization values (E_{corr}, I$_{corr}$, *Density*, R_p, *ΙΙp* and *CR*) of the prepared POM/ core-shell composites, their corresponding POMs and the core-shell as estimated from their Tafel plots. The polarization effect of CeO$_2$-TiO$_2$ core-shell on GCE According to our most recent data in **Figs. 16 and 17**, the corrosion potential (E_{corr}) of VO- > Mn- > Bi- > ZrO-> CoFe2O4@SiO2 composites is higher than that of CoFe2O4@SiO$_2$, and that of VO- >Bi -> Mn-> ZrO-> CeO$_2$@TiO$_2$ composites is higher than that of

CeO2@TiO$_2$ and of their respective POMS. The data obtained shows that the E_{corr} values of the composites are less negative than their POMS, indicating that they have more anticorrosive potential and **Figures 18 and 19** show the resulted Tafel curves for the bare SS and those coated with CoFe$_2$O$_4$@SiO$_2$ in addition to (A) includes those of ZrO-POM and ZrO-POM/ CoFe$_2$O$_4$@SiO$_2$ composites, (B) includes those of Mn-POM and Mn-POM/ CoFe$_2$O$_4$@SiO$_2$ composite. It is clear from Figs. 19 and 20 and data in Table 3 that the corrosion potential (I_{corr}) of the the ZrO-, Mn-, VO- and Bi- POMs/ CoFe$_2$O$_4$ @SiO$_2$ composites are 2.1 10^{-5} µA cm^{-2} and 5 10^{-5} µA cm^{-2}, 8.9 10^{-4} µA cm^{-2} and 2.6 10^{-4} µA cm^{-2} compared to 5.2 10^{-4} µA cm^{-2}, 0.008 µA cm^{-2}, 0.002 µA cm^{-2} and 0.003 µA cm^{-2} of their corresponding POMS respectively. Thus, the data obtained reveals that the I_{corr} of the composites are of more negative values compare to their POMS expressing their enhanced anticorrosive power. The I_{corr} values of the composites of the Bare steel, CoFe$_2$O$_4$@SiO$_2$ were found to 0.014 µA cm^{-2},

0.009 µA cm^{-2} be less negative compared to their corresponding M-POM/ CoFe$_2$O$_4$@SiO$_2$ respectively [31-33]. In addition to , it is shown in **Fig. 18** that after performing the corrosion test by immersion in 3.5% NaCl for one week (168 hrs) for Vo-POM/CoFe$_2$O$_4$@SiO$_2$, CoFe$_2$O$_4$@SiO$_2$ that Vo-POM/CoFe$_2$O$_4$@SiO$_2$ showed a very respectful anticorrosive potential.

The electrochemical equivalent circuit model used for EIS data fitting for the bare electrode and for the SS coated with M-POM/ CoFe2O4-SiO$_2$ epoxy system is presented in **Fig. 21.**

Furthermore, the Tafel experiments were carried-out to determine the effect of applying different paint coatings including various POM/CoFe$_2$O$_4$@SiO$_2$ composites and their corresponding POMs on the anodic dissolution of the SS and the cathodic reduction of the oxidant used. The Tafel plots of the bare SS plate and those coated with the ZrO-, Mn-, VO- and Bi-POMs

CoFe$_2$O$_4$@SiO$_2$ composites are shown in Figs 18 and 19. The values of the measured anodic Tafel slope (βa), cathodic Tafel slope (βc), corrosion current density (I_{corr}), corrosion rate (CR), corrosion efficiency [ηp] and the polarization resistance (R_p) of stainless steel electrodes coated with the same paint coatings are listed in Table 3.

The corrosion current (I_{corr}) was determined by drawing a straight line along the linear portion of cathodic or anodic curve and extrapolating it through E_{corr}. The corrosion rate is defined as the amount of corrosion loss (in thickness) per year (mm/year) and it was calculated using equation (6):

$$CR = (M\ I_{corr}/n\ D)\ x\ 3270 \quad (6)$$

where CR is the corrosion rate (mm/ Yr), I_{corr} is the corrosion density (µA /cm^2), D is the metal corroded density (gm/cm^3), and (M) molecular weight 55.85 g/mol for mild steel, n is 2 for the oxidation of steel, 3270 is a constant.

Table 3. Electrochemical corrosion data of uncoated SS plates and plates coated with paints containing core-shell CoFe$_2$O$_4$@SiO$_2$, POMs and their corresponding POMS/nano CoFe$_2$O$_4$@ SiO$_2$ composites measured before and after corrosion test in 3.5 % NaCl solution for three weeks at a scan rate 1mV/s.

Type of paint Property		Bare metal	CoF@S	ZrO-POM	ZrO-POM/CoF@S	Mn-POM	Mn-POM/CoF@S	Bi-POM	Bi-POM/CoF@S	VO-POM	VO-POM/CoF@S
I_{corr} density (µA cm^{-2})	B	0.014	0.009	5.25 × 10^{-4}	2.1 × 10^{-5}	0.008	5.0 × 10^{-5}	0.003	2.6 × 10^{-4}	0.0022	8.96 × 10^{-4}
	A	---	---	0.009	4.3 × 10^{-5}	0.012	0.002	0.011	8.7 × 10^{-4}	1.66	0.012
β_a (mV/d)	B	133.3	181.1	93.5	88.5	-37.5	-133.3	-55.2	68.4	214.3	-125
	A	-----		100	67.5	96.3	-100	76.9	-118.2	23	-180
$-\beta_c$ (mV/d)	B	97.5	166.6	115.6	190	250	94.6	57.2	200	68.2	222.2
	A	------	----	64	120	66.7	76	30.3	90.9	30	122.2
R_p (kΩ.cm^2)	B	1.75	4.2	4.32	124.9	1.7	48.6	4.06	8.52	10.22	3.88
	A	----	-----	1.78	43.9	1.42	9.38	0.86	2.56	0.0034	2.63
ηp (%)	B	----	35.7	96.3	97	40.7	96.4	76.7	81.5	83.7	93.6
	A	----	-----	31.6	96.9	16.6	85.7	24.2	38.2	0	14.8
CR, (mm/Yr)	B	159	102.7	59.1	2.4	94.4	5.7	34.1	29.5	25	102
	A	-----	------	108.1	4.9	136.4	22.7	125.1	98.8	-----	136.5

B: Before and A: After immersion in 3.5% Na Cl solution for three weeks, Measurements were done in 3.5% NaCl at a scan rate 1 mV/s . Abbreviations: CoF@S means CoFe$_2$O$_4$ @SiO$_2$

The corrosion efficiency [ηp] of an inhibitor is calculated from equation 8:

$$\eta p =(\ I_{corr\ uncoated} - I_{corr,\ coated}\ /\ I_{corr\ uncoated})\ x100 \quad (8)$$

Where $I_{corr,\ uncoated}$ and $I_{corr,\ coated}$ are the density of corrosion currents for uncoated and coated samples respectively.

Polarization resistance (R_p) is defined as the transition resistance between the electrode and the electrolyte. An electrode is polarized when its potential is displaced away from its equilibrium value at open circuit or corrosion potential. Polarization of an electrode causes current to flow due to electrochemical reactions induced at the electrode surface.

The polarization resistance (R_p) value can be calculated from equation (9):

$$R_p = \beta_a\ x\ \beta_c\ /\ 2.303\ (\beta a+ \beta_c)\ I_{corr}. \quad (9)$$

Data in Table 3 and Table 4 reveals that the E_{corr} of the paint containing POMs/CoFe$_2$O$_4$@SiO$_2$ composite goes for less negative values compared to those of MPOMs alone, i.e., for more noble character. The polarization resistance (R_P) obtained from Tafel measurements were calculated using Eq. (9). The results showed that there is a considerable increase in the polarization resistance of POMs/CoFe$_2$O$_4$@SiO$_2$ coating on SS substrate compared to those of bare SS, CoFe$_2$O$_4$@SiO$_2$ and M-POMs alone.

It is also obvious from Table 3 that the corrosion rate CR of the paint compositions containing ZrO and VO- POMS/ CoFe$_2$O$_4$ @SiO$_2$ were dramatically decreased compared to that of the bare, CoFe$_2$O$_4$@SiO$_2$ and POM- painted SS, while the CR values for Bi and VO -POM/ nano POMs/ CoFe$_2$O$_4$@SiO$_2$ were relatively improved. The significant decrease in I_{corr} and CR and the increase of E_{corr} of the POMs/ nano CoFe$_2$O$_4$ coating, may be

interpreted by the adsorption of the POMs/ nano CoFe₂O₄@SiO₂ on the surface of SS, forming a denser material. The dense arrangement of these materials makes the strength of the protective layer increase so that the corrosion rate decreases. It also implies that both the cathodic and anodic reactions are suppressed by the inhibitor/coating systems. Thus, it can be concluded that the inclusion of POMs/ $CoFe_2O_4@SiO_2$ nanocomposite into the paint coatings has dramatically enhanced its anticorrosion efficiency.

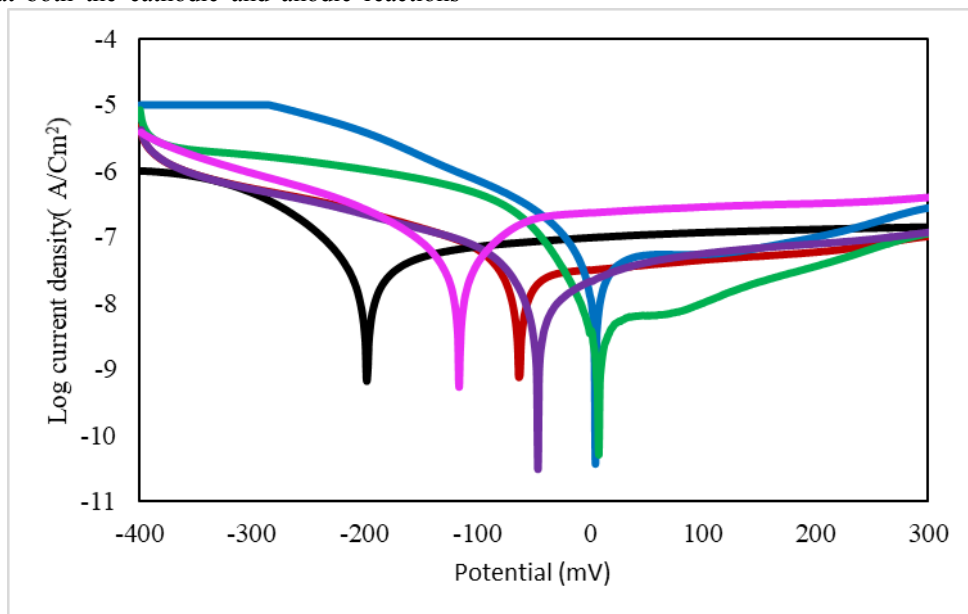**Fig. 16.** Tafel plot of bare electrode (black), $CeO_2@TiO_2$ core-shell (pink), ZrO-POM/ core-shell (violet), Mn-POM/ core-shell (red), VO-POM/ core-shell (green) Bi-POM/core-shell (blue) at a scan rate 1mV/s.
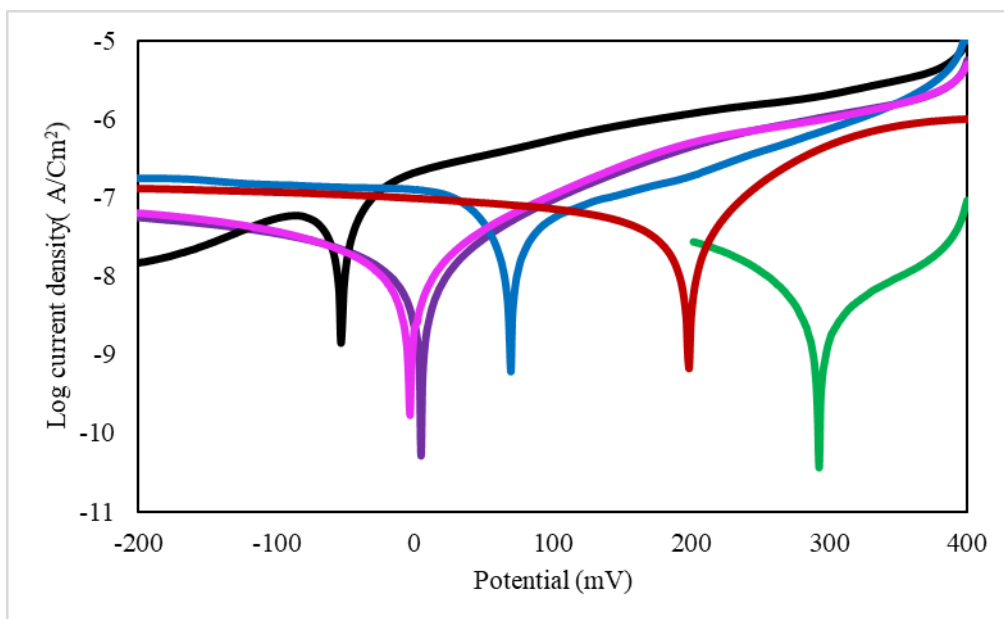

Fig. 17. Tafel plots of bare electrode GCE (black), $CoFe_2O_4@SiO_2$ (pink), ZrPOM/ core-shell (violet), MnPOM/ core-shell (red), VOPOM/ core-shell (green) and BiPOM/ core-shell (blue) at a scan rate 1mV/s measured in 3.5% NaCl solution.
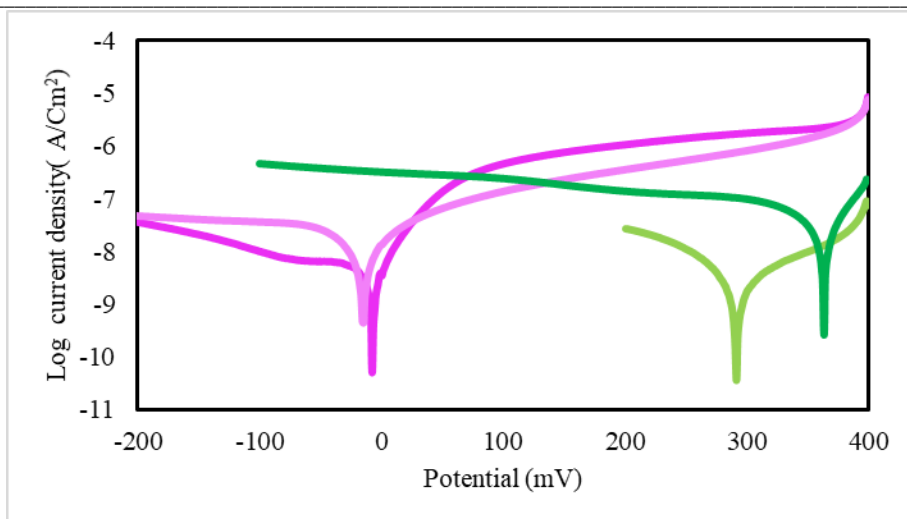
Fig. 18. Tafel plots at GCE for CoFe$_2$O$_4$@SiO$_2$ (pink), after one week (pale pink) VOPOM/ CoFe$_2$O$_4$@SiO$_2$ core-shell (green) and after 168 hours (pale green) in 3.5% NaCl .
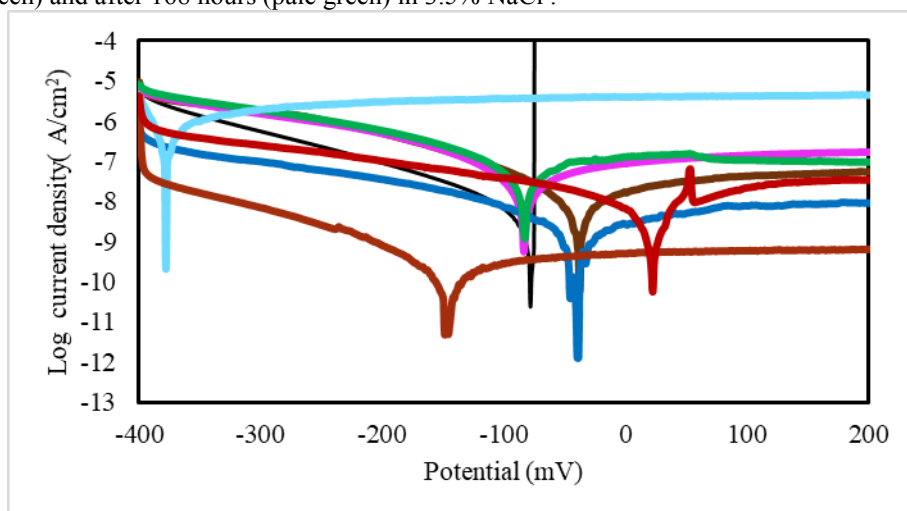

Fig. 19. Tafel plots of steel bare electrode (black), Blank epoxy-coated steel bar (brown), VO-POM/ CoFe2O4@SiO2 (red), VO-POM (blue) in 3.5% NaCl, and Vo-POM/ core-shell (green), VO-POM (light blue) and Blank epoxy-coated steel bar (light brown) after immersing in 3.5% NaCl for 3 weeks.
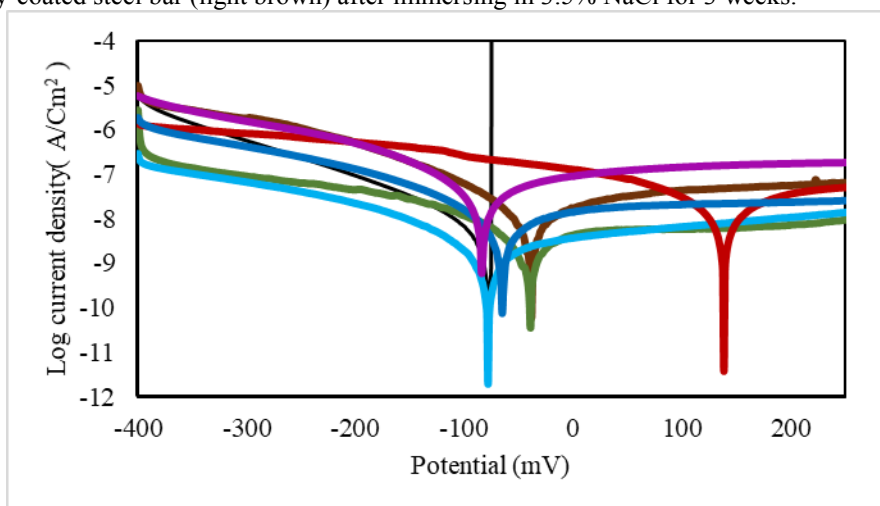
Fig. 20. Tafel plots of Bare electrode (black), Blank epoxy-coated steel bar (brown), CoFe$_2$O$_4$@SiO$_2$ (pink) Bi-CoFe$_2$O$_4$@SiO$_2$ (red), Bi-POM (blue) in 3.5% NaCl solution, and [Bi-POM/ core-shell (green), Bi-POM (light blue), (after immersing in 3.5% NaCl for 3 weeks).

Fig. 21. Electrochemical equivalent circuit model used for EIS data fitting (A) for Bare electrode, (B) for SS coated with M- POM/ CoFe2O4-SiO$_2$ epoxy.

4. Conclusion

This study showed that after three weeks immersion of the coated steel panels in 3.5% NaCl solution for the corrosion test, eco-friendly (ZrO, Mn, VO, and Bi) POM/CoFe$_2$O$_4$@SiO$_2$ nanocomposite coatings for stainless steel plates indicated enhanced electrical corrosion resistance performance. The electrochemical corrosion characteristics of the paint composites were greatly improved by the addition of CoFe$_2$O$_4$@SiO$_2$ nanoparticles. High anticorrosion performance of the composite coatings was confirmed by EIS evaluations. From the electrochemical studies, the results showed that:

1- The R_{ct} dramatically increased and the C_{dl} strongly decreased due to the adsorption of the metal-phosphomolybdate/ CoFe$_2$O$_4$ @ SiO$_2$ on the surface of stainless steel.

2- - The Tafel results are in agreement with the impedance results. The study confirmed the strong anticorrosion efficiency of the Zr=O, V=O POMs/cobalt ferrite@SiO$_2$ nano composites for the protection of mild stainless-steel substrates.

In conclusion, the protection mechanism for POM/CoFe$_2$O$_4$@SiO$_2$ nanocomposite coatings was governed by adsorption, and barrier effect due to the changes resulting from the formation of a more adhesion, denser and uniform layer on the steel surface. Initially, corrosive ions penetrate the coating and reach the surface of the steel, leading to anodic dissolution of the metal and a decrease in potential. Then, the nano-CoFe$_2$O$_4$@SiO$_2$ form a passive protective layer at the steel surface which inhibits the corrosion, and enhances the corrosion-protection efficiency of POM/CoFe$_2$O$_4$@SiO$_2$ nanocomposite coatings, as confirmed by EIS and potentiometric polarization study

References

[1] R. Winston Revie, H. H. Uhlig, Corrosion and Corrosion Control. An Introduction to Corrosion Science and Engineering Fourth Edition (2008) by John Wiley & Sons, Inc. All right reserved Published by John Wiley & Sons, Inc., Hoboken New Jersey.

[2] M.A.A. El-Ghaffar, E.A.M. Youssef, W.M. Darwish, F.M. Helaly, A novel series of corrosion inhibitive polymers for steel protection, Journal of Elastomers & Plastics 30 (1998) 68-94

[3] A.S. Fouda, M.A.A. El-Ghaffar, M.H. Sherif, A.T. El-Habab, A. El-Hossiany, Novel Anionic 4-Tert-Octyl Phenol Ethoxylate Phosphate Surfactant as Corrosion Inhibitor for C-steel in Acidic Media Protection of Metals and Physical Chemistry of Surfaces 2020 (2019)1-13.

[4] M. A. Abd El-Ghaffar, A. M. Baraka, M. M. Hefny, E. A. Youssef and Mahmoud M. Aly, Boron Phosphate/Poly(p-phenylenediamine) as a Corrosion Inhibitive System for Steel Protection, Egypt. J. Chem., 61(2018) 759 – 771

[5] M. A. Abd El-Ghaffar, Nivin M. Ahmed, E.A.M. Youssef, High performance anticorrosive paint formulations based on phosphate pigments, Pigment and Rein Technology, 33, No.4 (2004), 226-237

[6] A. El Nemr, A Elhebshi, M. S. El-Deab, I. Ashour, S.Ragab, Synergistic Effect of Chitosan Biguanidine Hydrochloride Salt as a Green Inhibitor for Stainless Steel Alloy Corrosion in a 0.5 M H2SO4 Solution, Egypt. J. Chem. 65, (2022) 389 – 398.

[7]. G. Koch, J. Varney, N. Thompson, O. Moghissi, M. Gould, J. Payer, International Measures of Prevention, Application, and Economics of Corrosion Technologies Study, Houston, (2016).

[8] M.A. Abd El-Ghaffar, N.A. Abdelwahab, A. M. Fekry, M.A. Sanad, M.W. Sabaa, S.M.A. Soliman, Polyester-epoxy resin / conducting polymer / barium sulfate hybrid composite as a smart eco-friendly anti-corrosive powder coating, Progress in Organic Coatings, 144 (2020) 105664.

[9] (a) M.A. Abd El-Ghaffar , N.A. Abdelwahab , Amany M. Fekry , M.A. Sanad , M.W. Sabaa , S.M.A. Soliman , Polyester-epoxy resin/conducting polymer/barium sulfate hybrid composite as a smart eco-friendly anti-corrosive powder coating,Progress in Organic Coatings 144 (2020) 105664. (b) Z. Tao, S. Zhang, W. Li, B. Hou, Corrosion inhibition of mild steel in

acidic solution by some oxo-triazole derivatives, Corros. Sci. 51 (2009) 2588–2595

[10] M. A. Abd EL-Ghaffar, E.A, Youssef, N. M. Ahmed, Preparation and characterisation of high performance yellow anticorrosive phosphomolybdate pigments, Pigment & resin technology, 35(2006) 3522-29.

[11] D. R. Mohammedali, H. I. Salman1, M. N. Bahjat1, E. S. Abood, Synthesis of new Corrosion Inhibitor from Nano-Polymer and study its adsorption on carbon steel at different Temperatures, Egypt. J. Chem. 65(2022) 691-705.

[12] Zheludkecich, M.L.; Salavado, I.M.; Ferreira, M.G.S. Sol-gel coatings for corrosion protection of metals. J. Mater. Chem. 15 (2005) 5099–5111.

[13] Montemor, M.; Pinto, R.; Ferreira, M.G.S. Chemical composition and corrosion protection of silane films modified with CeO2 nanoparticles. Electrochim. Acta 54 (2009) 5179–5189.

[14] Venila, R.; Kamaraj, P.; Arthanareeswari, M.; Devikala, S. Surface modification of mild steel using Ag doped SnO2 nanoparticles for corrosion inhibition. Int. J. Adv. Chem. Sci. Appl. 1 (2014) 16–20.

[15] Deyab, M.A.; Keera, S.T. Effect of nano- TiO2 particles size on the corrosion resistance of alkyd coating. Mater. Chem. Phys. 146(2014) 406–411.

[16] Shi, X.; Nguyen, T.A.; Suo, Z.; Liu, Y.; Avci, R.A. Effect of nanoparticles on the anticorrosion and mechanical properties of epoxy coating. Surf. Coat. Technol. 204(2009) 237–245.

[17] Zand, R.Z.; Verbeken, K.; Adriaens, A. Influence of the cerium concentration on the corrosion performance of Ce-doped silica hybrid coatings on hot dip galvanized steel substrates. Int. J. Electrochem. Sci. 8(2013) 548–563.

[18] M. A. Abd El-Ghaffar, N. M. Ahmed, E. A. Youssef, A method for preparation and application of micronized ferrite pigments in anticorrosive solvent-based paints, Journal of Coatings Technology and Research, 7 (2010) 703-713.

[19] G.X. Shen, Y.C. Chen, C.J. Lin, Corrosion protection of 316 L stainless steel by a TiO2 nanoparticle coating prepared by sol-gel method, Thin Solid Films. 489(2005) 130-136. https://doi.org/10.1016/j.tsf.2005.05.016

[20] M.G. Mahmoud, R. Wang, M. Kato, K. Nakasa, Influence of ultraviolet light irradiation on corrosion behaviour of weathering steel with and without TiO2-coating in 3mass% NaCl solution, Scr. Mater. 53(2005)1303-1308. https://doi.org/10.1016/j.scriptamat.2005.07.039.

[21] Z. Yu, H. Di, Y. Ma, Y. He, L. Liang, L. Lv, X. Ran, Y. Pan, Z. Luo, Preparation of graphene oxide modified by titanium dioxide to enhance the anti-corrosion performance of epoxy coatings, Surf. Coatings Technol. 276(2015)471-478. https://doi.org/10.1016/j.surfcoat.2015.06.027.

[22] S.Narsingam, B. Satish, V. Rao.Kalagadda Synthesis and Characterization of Ceria-Titania (CeO2 - TiO2) Core-Shell Nanoparticles for Enzymatic Bio Sensing Application, Current Nanomaterials, 1(2016) 132-138[23]Ref.23

[23] M. Gharagozlou,Influence of calcination temperature on structural and magnetic properties of nanocomposites formed by Co-ferrite dispersed in sol-gel silica matrix using tetrakis(2-hydroxyethyl) orthosilicate as precursor Chemistry Central Journal 5(2011)19

[24] (a) J. Wang, Y. Qi, X. Zhao, Z. Zhang, Electrochemical Investigation of Corrosion Behavior of Epoxy Modified Silicate Zinc-Rich Coatings in 3.5% NaCl Solution, Coatings, 10 (2020) 444. (b) M. Birdeanu, I. Fratilescu, C. Epuran, A. C. Murariu, G. Socol and E. Fagadar-Cosma Efficient Decrease in Corrosion of Steel in 0.1 M HCl Medium Realized by a Coating with Thin Layers of MnTa2O6 and Porphyrins Using Suitable Laser-Type Approaches. Nanomaterials 12(2022) 1118. https://doi.org/10.3390/nano12071118

[25] (a) M. Mobin , F. Ansar, Polythiophene (PTh)−TiO2−Reduced Graphene Oxide (rGO) Nanocomposite Coating: Synthesis, Characterization, and Corrosion Protection Performance on Low-Carbon Steel in 3.5 wt % NaCl Solution, ACS Omega 7(2022) , 46717−46730. (b) S.A.X. Stango, U. Vijayalakshmi, Studies on corrosion inhibitory effect and adsorption behaviour of waste materials on mild steel in acidic medium, J, Asian, Ceram, Soc., 6(2018) 20-29.

[26] S. A. Haddadi, M. Mahdavian, E. Karimi, Evaluation of the corrosion protection properties of an epoxy coating containing sol–gel surface modified nano-zirconia on mild steel. RSC Advances, 5 (2015), 28769–28777.

[27] W. Al Zoubi and Y. Gun Ko, Enhanced Corrosion Protection Performance by Organic-Inorganic Materials Containing Thiocarbonyl Compounds. Scientific Report 8 (2018) 10925.

[28] B. M. Singh Bisht, H. Bhandari, P. Sambyal, S. P. Gairola, S. K. Dhawan, Highly Durable and Novel Anticorrosive Coating Based on Epoxy Reinforced with Poly(Aniline-co-Pentafluoroaniline)/SiO2 Composite. American Journal of Polymer Science 6 (2016) 75-85.

[29] H.H. Hassan, Inhibition of mild steel corrosion in hydrochloric acid solution by triazole derivatives: Part II: Time and temperature effects and thermodynamic treatments, Electrochem. Acta, 531(2007) 1722–1730.

_____

[30] D.K. Yadav, M.A. Quraishi, B. Maiti, Inhibition effect of some benzylidenes on mild steel in 1M HCl: An experimental and theoretical correlation, Corros. Sci., 55(2012) 254–266.

[31] Y.H. Fang, Z.P. Liu, Mechanism and Tafel lines of electro-oxidation of water to oxygen on RuO2 (110), J. Am. Chem. Soc., 132 (2010) 18214–18222.

[32] M. Erna, H. Herdini, and D. Futra Corrosion Inhibition Mechanism of Mild Steel by Amylose-Acetate/Carboxymethyl Chitosan Composites in Acidic Media, Hindawi, International Journal of Chemical Engineering (2019).

[33] S. Arul Xavier Stango and U. Vijayalakshmi, Studies on corrosion inhibitory effect and adsorption behaviour of waste materials on mild steel in acidic medium, JOURNAL OF ASIAN CERAMIC SOCIETIES,6 (2018) 20–29.

_____